



Reactive belite stabilization mechanisms by boron-bearing dopants

Ana Cuesta^a, Enrique R. Losilla^a, Miguel A.G. Aranda^a, Jesús Sanz^b, Ángeles G. De la Torre^{a,*}

^a Departamento de Química Inorgánica, Cristalografía y Mineralogía, Universidad de Málaga, 29071-Málaga, Spain

^b Instituto de Ciencia de Materiales de Madrid (ICMM), Consejo Superior de Investigaciones Científicas (CSIC), Cantoblanco, 28049 Madrid, Spain

ARTICLE INFO

Article history:

Received 11 August 2011

Accepted 27 January 2012

Keywords:

Crystal Structure (B)

X-Ray Diffraction (B)

Ca₂SiO₄ (D)

Solid solution

Active belite cements

ABSTRACT

Belite-rich cements hold promise for reduced energy consumption and CO₂ emissions, but their use is hindered by the slow hydration rates of ordinary belites. This drawback may be overcome by activation of belite by doping. Here, the doping mechanism of B and Na/B in belites is reported. For B-doping, three solid solutions have been tested: Ca_{2-x/2}□_{x/2}(SiO₄)_{1-x}(BO₃)_x, Ca₂(SiO₄)_{1-x}(BO₃)_xO_{x/2} and Ca_{2-x}B_x(SiO₄)_{1-x}(BO₄)_x. The experimental results support the substitution of silicate groups by tetrahedral borate groups with the concomitant substitution of calcium by boron for charge compensation, Ca_{2-x}B_x(SiO₄)_{1-x}(BO₄)_x. Otherwise, the coupled Na/B-doping of belite has also been investigated and Ca_{2-x}Na_x(SiO₄)_{1-x}(BO₃)_x series is confirmed to exist for a large range of x values. Along this series, α_H-C₂S is the main phase (for x ≥ 0.10) and is single phase for x = 0.25. Finally, a new structural description for borax doping in belite has been developed for α_H-Ca_{1.85}Na_{0.15}(SiO₄)_{0.85}(BO₃)_{0.15}, which fits better borax activated belite cements in Rietveld mineralogical analysis.

© 2012 Elsevier Ltd. All rights reserved.

1. Introduction

The manufacture of Portland cement on average emits about 0.83 tons of CO₂ per tonne of cement, which is not particularly high for a chemical product. However, because of the enormous volumes of cement used worldwide to make concrete, such emissions amount to about 6% of all anthropogenic CO₂ emissions [1]. Cements based on belite have been proposed as environmentally friendly materials, as the reduction of CO₂-emissions may be as much as 10% for belite Portland cements [2–4] or up to 35% in belite calcium sulfoaluminate cements [5,6]. Belite Portland cements are being already used in “low heat hydration concretes” for construction of large dams and lining of oil wells. However, the massive application of these materials requires the overcoming of some drawbacks such as the low hydration rate of the belite phase and high resistance to be milled [7,8]. Belite calcium sulfoaluminate cements are also being partially used in China [6,9].

Belite (Ca₂SiO₄, C₂S, with some substituting elements) is the major constituent of Belite Portland cements and some calcium sulfoaluminate cements. Currently, borate-activated belite calcium sulfoaluminate cements are undergoing industrial trials under an EU project (<http://www.aether-cement.eu/>) to determine the CO₂ savings. Furthermore, this phase is also the second most abundant constituent of OPC [10]. Stoichiometric C₂S has five polymorphs [11,12] (γ, β, α_L, α_H and α) and its temperature evolution is shown in Fig. 1. The

γ-phase, which is essentially nonreactive with water, is stable at ambient temperature and it crystallizes in an orthorhombic olivine-type structure [13–15]. The β-form is a metastable monoclinic phase at room temperature [16,17]. α_L and α_H orthorhombic phases are stable at higher temperatures [18]. The α_L-polymorph is generally considered a superstructure of the α_H and it has been reported two possibilities for indexing: doubling the *a* and *c* parameters [19] or tripling the *b* parameter [20–22]. Finally, the highest-temperature polymorph is the α-form whose structure is still under discussion [23–25]. It is noteworthy, that β → γ polymorphic transformation on cooling is disruptive with a change of 12 vol%. This effect, called “dusting”, causes the material to disintegrate spontaneously to a powder [26] and can be avoided by chemical, thermal and mechanical treatments [10,11].

The framework of silicon tetrahedra is very similar among these polymorphs, while the arrangement of calcium cations is slightly different. The crystal structure of γ-C₂S has two calciums in regular six-coordinated oxygen environments. Meanwhile, the crystal structure of β-C₂S has two calciums surrounded by eight oxygens in distorted environments. Furthermore, the crystal structures of α_H- and α-polymorphs have calcium cations in both eight and nine irregular coordinations [11–16]. It is worth noting that there are experimental evidences that an increase of the calcium coordination number seems to enhance the water reactivity [27]. However, the actual reactivity of each form depends on the kind and amount of dopants employed [28–30]. Therefore, theoretical calculations [31] are needed to properly address this issue.

It is known that the presence of defects or strains in crystalline structures can modify physical and chemical properties, or even

* Corresponding author. Tel.: +34 952131877; fax: +34 952131870.
E-mail address: mgd@uma.es (Á.G. De la Torre).

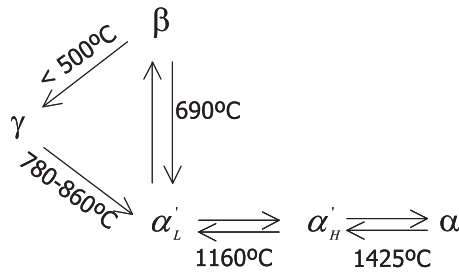


Fig. 1. Polymorphic transformations of stoichiometric Ca_2SiO_4 with temperature.

causes the stabilization of a high temperature form at room temperature [32,33]. The different type of defects (overall known as microstrains) can be introduced during the material preparation by the formation of solid solutions or by specific thermal treatments [34]. The effects on chemical-stabilizing ions on the stability of β - C_2S have been extensively investigated [11,28,35], and several theoretical predictions have been made about which ions can stabilize β - C_2S (B_2O_3 , Na_2O , K_2O , BaO , MnO_2 , Cr_2O_3 or their combinations) [29,36–39]. It has been published that foreign oxides, such as MgO , P_2O_5 , K_2O , BaO and SO_3 , promote the formation of α' - C_2S and increase its hydraulic properties [40,41]. B_2O_3 has also been studied in order to stabilize β - C_2S and α' - C_2S at room temperature [28,42]. Some authors [27,42,43] have demonstrated that the effectiveness of addition of B_2O_3 , with no other co-dopants, for stabilizing for α' -forms, is poor. On the other hand, the addition of a combination of dopants, for instance, B_2O_3 and Na_2O , successes to stabilize α' - C_2S [42] although these authors did not state which α' -forms, α'_L or α'_H , was stabilized. Moreover, previous studies reported that borax stabilizes α' -form in a cement matrix [5]. The α - C_2S is much more difficult to stabilize at room temperature, however this phase was stabilized by the addition of alkaline oxides in belite Portland cements [44,45].

The objective of this study is to investigate the mechanism of α' -belite stabilization at room temperature by B_2O_3 and Na_2O additions. An improved structural description of α'_H - C_2S polymorph is reported. The driving force for this research is the need to manufacture, and to understand the production, of highly reactive belite calcium sulfoaluminate cements. The final goal is the need to reduce CO_2 emissions in the cement industry.

2. Experimental section

2.1. Sample preparation

Two types of C_2S series have been synthesized. The first type deals with the C_2S stabilization just by boron doping. Three solid solutions with nominal stoichiometries $\text{Ca}_{2-x/2}\text{B}_{x/2}(\text{SiO}_4)_{1-x}(\text{BO}_3)_x$, $\text{Ca}_2(\text{SiO}_4)_{1-x}(\text{BO}_3)_x\text{O}_{x/2}$ and $\text{Ca}_{2-x}\text{B}_x(\text{SiO}_4)_{1-x}(\text{BO}_4)_x$ have been tested. In this case, the boron source was boric acid. The second type of series deals with the C_2S stabilization by boron and sodium doping. Two solid solutions with nominal stoichiometries $\text{Ca}_{2-x}\text{Na}_x(\text{SiO}_4)_{1-x}(\text{BO}_3)_x$ and $\text{Ca}_{2-3x}\text{B}_{2x}\text{Na}_x(\text{SiO}_4)_{1-x}(\text{BO}_4)_x$ have been tested. For these solid solutions, borax was used as main dopant source but sodium carbonate and boric acid were also added as correctors to achieve the right stoichiometries for the first and second series, respectively.

All series were prepared using CaCO_3 (99.95%–100.05% from Alfa Aesar) and SiO_2 (99.7% from ABCR). Dopants were added as H_3BO_3 (100% from VWR), $\text{Na}_2\text{B}_4\text{O}_7 \cdot 10\text{H}_2\text{O}$ (100% from Aldrich) and Na_2CO_3 (99.999% from Aldrich). Table 1 shows the nominal elemental composition expressed as oxides for each member of each solid solution, excluding CO_2 and H_2O . Raw mixtures were ground for 10 min in an agate mortar with acetone, and preheated at 1000 °C for 4 hours (heating rate of 10 °C/min) in Pt/Rh crucibles. Mixtures were placed on Pt/Rh crucibles and preheated at 1000 °C for 4 hours (heating

Table 1

Nominal elemental composition expressed in weight percentages of oxides for each member of the proposed Ca_2SiO_4 solid solutions.

Nominal stoichiometry	x	CaO	SiO ₂	B ₂ O ₃	Na ₂ O
Ca₂SiO₄	0.00	65.12	34.88	–	–
Ca_{2-x/2}B_{x/2}(SiO₄)_{1-x}(BO₃)_x	0.025	65.22	34.28	0.51	–
	0.10	65.52	32.40	2.09	–
	0.025	65.36	34.14	0.51	–
Ca₂(SiO₄)_{1-x}(BO₃)_xO_{x/2}	0.10	66.09	31.86	2.05	–
	0.0125	64.93	34.56	0.51	–
	0.01875	64.83	34.40	0.76	–
Ca_{2-x}B_x(SiO₄)_{1-x}(BO₄)_x	0.025	64.74	34.24	1.02	–
	0.05	64.36	33.59	2.05	–
	0.10	63.58	32.27	4.15	–
	0.15	62.78	30.90	6.32	–
	0.20	61.95	29.50	8.55	–
	0.025	64.78	34.26	0.51	0.45
	0.05	64.43	33.63	1.03	0.91
	0.10	63.72	32.34	2.08	1.85
Ca_{2-3x}B_{2x}Na_x(SiO₄)_{1-x}(BO₄)_x	0.15	63.00	31.01	3.17	2.82
	0.20	62.24	29.64	4.29	3.82
	0.25	61.47	28.23	5.45	4.85
	0.025	63.53	34.48	1.54	0.46
	0.05	61.90	34.06	3.11	0.92
	0.10	58.51	33.18	6.41	1.90

rate of 10 °C/min). After cooling, the mixtures were milled with 2-butanol in a Fritsch ball mill (model Pulverisette 7, 45 cm³ agate vessel containing 7 agate balls with a diameter of 15 mm) during 1 h at 100 rpm with reverse rotation each 20 min, and dried at 100 °C in a stove. The resulting powders were pelletized (20 mm diameter) and a second thermal treatment was carried out at 1300 °C for 30 min (heating rate of 20 °C/min) and quenched from high temperature with an air flow. The pellets were broken and grounded in WC mortar. The resulting powders were characterized by the techniques described below.

Finally, a laboratory-prepared iron-rich belite calcium sulfoaluminate clinker has also been prepared. This clinker was activated by adding borax ($\text{Na}_2\text{B}_4\text{O}_7 \cdot 10\text{H}_2\text{O}$) (2.0 wt% expressed as B_2O_3) to the raw material to promote room temperature stabilization of reactive belite polymorph (α'_H -form). The preparation and full characterization, including Rietveld quantitative phase analysis, has been already reported [5]. This clinker contains 56.7 wt% of α'_H - C_2S , 31.1 wt% of $\text{C}_4\text{A}_3\text{S}$, 10.1 wt% of C_4AF and 2.1 wt% of CT and it is hereafter named BCSAF-B2.

2.2. X-ray powder diffraction

All members of the C_2S solid solutions were characterized by laboratory X-Ray powder diffraction (LXRPD). Diffraction data were recorded on an X'Pert MDP PRO diffractometer (PANalytical) equipped with a Ge (111) primary monochromator, using monochromatic $\text{CuK}\alpha_1$ radiation ($\lambda = 1.54059 \text{ \AA}$) and an X'Celerator detector. The overall measurement time was ~4 h per pattern to have good statistics over the 5.0° to 140.0° (2 θ) angular range, with 0.017° step size.

2.3. Rietveld analysis

All Rietveld quantitative phase analyses (RQPA) were carried out using the GSAS suite of programs [46]. Final global optimized parameters were: background coefficients, zero-shift error, cell parameters and peak shape parameters using a pseudo-Voigt function [47] corrected for axial divergence [48]. $\text{Ca}_{1.85}\text{Na}_{0.15}(\text{SiO}_4)_{0.85}(\text{BO}_3)_{0.15}$ sample patterns were used to obtain an improved structural description for doped α'_H - C_2S polymorph. In this case, the atomic positional coordinates and isotropic atomic displacement parameters (ADP) were optimized.

2.4. Infrared spectroscopy

ATR-FTIR (Attenuated Total Reflectance – Fourier Transform Infrared) spectra were obtained with an ATR accessory (MIRacle ATR, PIKE Technologies, USA) coupled to FTIR spectrometer (FT/IR-4100, JASCO, Spain). All spectra were recorded in the 4000 to 600 cm⁻¹ range at 4 cm⁻¹ resolution and 25 scans were accumulated. The powder samples were placed on a holder of approximately 3 mm of diameter.

2.5. ¹¹B Magic Angle Spinning Nuclear Magnetic Resonance (MAS NMR)

¹¹B (I = 3/2) MAS-NMR spectra for three selected samples were recorded in an Avance-400 Bruker spectrometer. The resonance frequency was 128.38 MHz (B₀ = 9.4 T). Spectra were recorded using $\pi/2$ (5 μ s) pulses and 5 s intervals between accumulations with the spinning rate of samples being 10 kHz. In all cases, spectral filters used were 125 kHz and the appropriate number of scans was chosen in order to obtain S/N ratios higher than 30. Measurements were done at room temperature with boric acid as external reference. The error in chemical shift values is estimated to be lower than 0.5 ppm.

2.6. Scanning electron microscopy

Small pellets with cylindrical shape for selected compositions were studied in a JEOL JSM-6490LV scanning electron microscope using secondary electrons. EDX measurements were carried out with the OXFORD INCA Energy 350 attachment. This unit has a Si(Li) detector with a super atmospheric thin window (SATW). Samples were coated with graphite.

2.7. Inductively coupled plasma mass spectroscopy

The elemental compositions of samples, after the thermal treatments, were determined by ICP-MS on Perkin Elmer spectrophotometer (Nexion 300D). Previously, samples were digested in an Anton Paar device (Multiwave 3000) by using HNO₃, HCl and HF.

3. Results and discussion

3.1. Solid solution mechanisms

Previous studies have shown that boron is an effective dopant in belite to stabilize the β -polymorph [27,43] and even higher temperature polymorphs [28,42]. Furthermore, there is a report mentioning that boron is incorporated in belite as BO₄⁵⁻ [11]. However, there is not reported mechanism for the boron incorporation within belites. The first issue to be addressed is the boron anion nature within belites, i.e. if the borate group is tetrahedral BO₄⁵⁻ or planar-triangular BO₃³⁻. Furthermore, as the B-doping in the silicate framework, SiO₄⁴⁻, is aliovalent, it is also a key point to understand the charge compensating mechanism. In order to address these open issues, three nominal solid solutions have been tested: i) Ca_{2-x/2}□_{x/2}(SiO₄)_{1-x}(BO₃)_x; ii) Ca₂(SiO₄)_{1-x}(BO₃)_xO_{x/2}; and iii) Ca_{2-x}B_x(SiO₄)_{1-x}(BO₄)_x (see Table 1). The first two series are designed for stabilizing with planar-triangular BO₃³⁻ anions. The first one is charge compensated with calcium vacancies and the second with interstitial oxide anions, as in other silicate-based systems [49]. Table 2 shows RQPA results for these two series and chiefly, all members contain large amounts of free calcium oxide, which indicate that the target compositions were not achieved. Furthermore, ATR-FTIR infrared spectra of these two series, Figures S1 and S2, show the presence of BO₃³⁻ units but also BO₄⁵⁻-type groups, characteristic vibrations close to 1250 cm⁻¹ and 1000 cm⁻¹, respectively [50,51]. The BO₄⁵⁻ vibration at 1000 cm⁻¹ is overlapped with that arising from SiO₄⁴⁻. The third mechanism is based on substitution of tetrahedral SiO₄⁴⁻ groups by tetrahedral BO₄⁵⁻ units with concomitant boron substitution of calcium for

Table 2

Rietveld quantitative phase analyses for each member of the proposed Ca₂SiO₄ solid solutions.

Stoichiometry	Nominal value x	γ -C ₂ S	β -C ₂ S	α' -C ₂ S	CaO
Ca₂SiO₄	0.00	58.9(1)	41.1(1)	-	-
Ca_{2-x/2}□_{x/2}(SiO₄)_{1-x}(BO₃)_x	0.025	3.6(3)	89.2(1)	3.4(3)	3.7(2)
	0.10	3.9(6)	58.2(6)	33.1(8)	4.8(3)
Ca₂(SiO₄)_{1-x}(BO₃)_xO_{x/2}	0.025	3.0(3)	89.8(1)	3.7(3)	3.5(2)
	0.10	3.1(6)	59.9(6)	32.9(7)	4.1(3)
Ca_{2-x}B_x(SiO₄)_{1-x}(BO₄)_x	0.0125	1.9(1)	95.5(1)	2.0(1)	0.7(1)
	0.0187	0.9(1)	83.4(1)	15.6(4)	-
	0.025	0.8(1)	77.1(1)	22.2(4)	-
	0.05	0.7(1)	65.5(2)	33.8(3)	-
	0.10	0.6(1)	15.9(3)	83.5(1)	-
Ca_{2-x}Na_x(SiO₄)_{1-x}(BO₃)_x	0.025	36.4(1)	56.6(2)	6.9(2)	-
	0.05	17.0(2)	56.3(2)	26.7(3)	-
	0.10	-	41.8(2)	58.2(1)	-
	0.15*	-	9.9(2)	90.1(1)	-
	0.20	-	8.4(3)	91.6(1)	-
	0.25	-	-	100.0(-)	-
Ca_{2-3x}B_{2x}Na_x(SiO₄)_{1-x}(BO₄)_x	0.025 [#]	0.3(1)	69.2(1)	23.8(3)	-
	0.05 [§]	0.5(1)	6.9(4)	67.2(1)	-

* Sample used for the structural study of α' -C₂S. [#] It also contains 6.7(2) wt% of Ca₃Si₂O₇. [§] It also contains 25.5(2) wt% of Ca₃Si₂O₇.

charge compensation, Ca_{2-x}B_x(SiO₄)_{1-x}(BO₄)_x (0 ≤ x ≤ 0.20). This mechanism is similar to that already reported for aluminum doping in alite, Ca_{3-x}Al_x(SiO₄)_{1-x}(AlO₄)_xO [52]. Samples with x = 0.15 and x = 0.20 of this series were melted at high temperature, thus these compositions were not further studied. Fig. 2 shows raw LRPD patterns for the Ca_{2-x}B_x(SiO₄)_{1-x}(BO₄)_x series, up to x = 0.10, with diagnostic peaks labelled in order to identify a given polymorph. Table 2 gives RQPA for all members up to x = 0.10 of this series and it shows that the amount of CaO is, for all these x values, lower than 1.0 wt%. Moreover, Table 2 shows that for x = 0.00 β -polymorph has been partially stabilized, being mainly due to the milling processes performed to raw materials and to the quenching. The polymorph β -C₂S is present as main phase, i.e. more than 60.0 wt% up to x = 0.05, meanwhile α' -C₂S is the main phase for x = 0.10. Moreover, ATR-FTIR infrared spectra were also performed and Fig. 3a shows the ATR-FTIR infrared spectra of all the members of this series (up to x = 0.10). These measurements show bands close to 1000 cm⁻¹ assigned to BO₄⁵⁻ stretching vibrations. Furthermore, tiny signals from 1150 to 1350 cm⁻¹, corresponding to BO₃³⁻ (or similar) units, are also observed (see Fig. 3a) [50,51]. However, these results do not rule out the formation of this series due to the fact that BO₃³⁻ units (or quite similar groups) can be locally formed where boron cations substitute calcium atoms. Boron is much smaller than calcium and a large displacement within the site is expected which may lead to the formation of a BO₃³⁻-type groups. Variation of the unit cell volume in this solid solution is given in Fig. 4 (open symbols) and final refined unit cell values are included in Table S1, as supplementary material. It is relevant that γ -form unit cell volume is constant in its whole chemical field of existence, i.e. dopants are not incorporated within γ -C₂S. On the other hand, β - and α' -form unit cell volumes are relatively constant up to x = 0.0125 and decrease for higher values of x. Taking all these results into account, it can be stated that boron stabilizes high temperature polymorphs by substituting jointly silicon units as BO₄⁵⁻ and calcium cations by B³⁺, as for aluminum doping in alite [52].

On the other hand, borax is a relatively inexpensive raw material for boron (and sodium) doping in belite cements and it is already being used in industrial trials. Furthermore, it is known to stabilize high-temperature forms of belite [12,53–55]. Unfortunately, there are not reports dealing with the charge compensating mechanism for borax, i.e. B and Na, stabilization of belite. As it was discussed above, two possibilities for borate incorporation arises, BO₄⁵⁻ or BO₃³⁻.

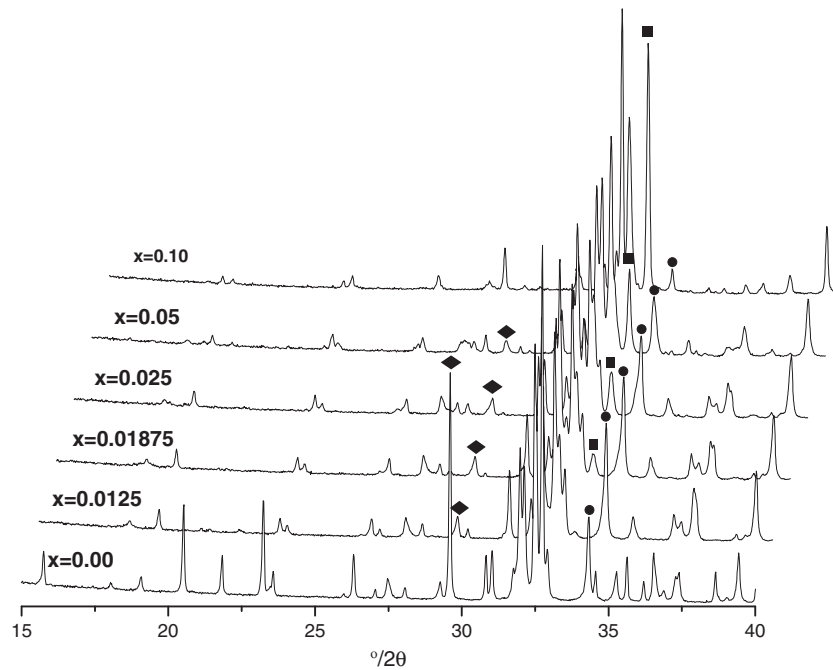


Fig. 2. 3D-view of a selected range of the LXRDP patterns for $\text{Ca}_{2-x}\text{B}_x(\text{SiO}_4)_{1-x}(\text{BO}_4)_x$ solid solution. Symbols highlight diagnostic peaks for $\gamma\text{-C}_2\text{S}$ (rhombus); $\beta\text{-C}_2\text{S}$ (circle) and $\alpha'\text{-H-C}_2\text{S}$ (square).

Therefore, two solid solutions were tested using boron and sodium as dopants: i) $\text{Ca}_{2-x}\text{Na}_x(\text{SiO}_4)_{1-x}(\text{BO}_3)_x$; and ii) $\text{Ca}_{2-3x}\text{B}_{2x}\text{Na}_x(\text{SiO}_4)_{1-x}(\text{BO}_4)_x$. In addition to borax, sodium carbonate and boric acid were also added as correctors for achieving the right doping contents, for the first and second solid solutions, respectively. Fig. 5 shows raw

LXRDP patterns for the $\text{Ca}_{2-x}\text{Na}_x(\text{SiO}_4)_{1-x}(\text{BO}_3)_x$ series with diagnostic peaks labelled in order to identify a given polymorph and Table 2 gives RQPA of this series. The first result shown in Table 2 is the absence of free calcium oxide along this series. A second very relevant result is that high temperature polymorphs of C_2S , i.e. $\beta\text{-}$ and $\alpha'\text{-H-C}_2\text{S}$, are stabilized as x increases, as expected. Elemental analysis by ICP-MS was performed for all the members of this series to determine the volatilization rate of sodium, see Table S2. The sodium losses, expressed as Na_2O wt%, represented 34% of the total at the lowest Na_2O addition rate but only 15% at the highest addition rate. Therefore, used nominal compositions do not fully represent the stoichiometry of the bulk phases. Furthermore, B_2O_3 contents were also analysed by ICP-MS for the $\text{Ca}_{2-x}\text{B}_x(\text{SiO}_4)_{1-x}(\text{BO}_4)_x$ and $\text{Ca}_{2-x}\text{Na}_x(\text{SiO}_4)_{1-x}(\text{BO}_3)_x$ series. The measured volatilization rates were negligible with retention rates larger than 95%.

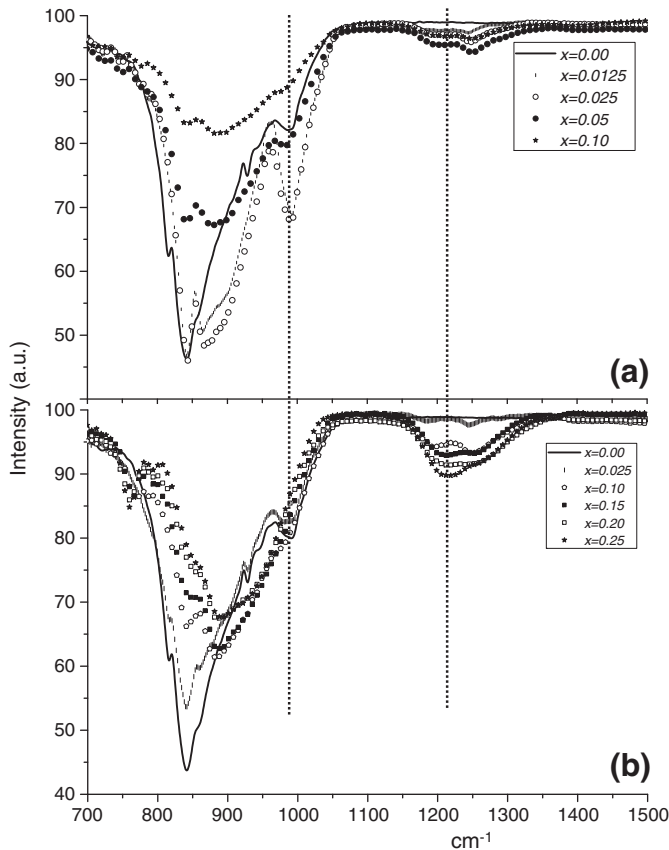


Fig. 3. ATR-FTIR infrared spectra for (a) $\text{Ca}_{2-x}\text{B}_x(\text{SiO}_4)_{1-x}(\text{BO}_4)_x$ and (b) $\text{Ca}_{2-x}\text{Na}_x(\text{SiO}_4)_{1-x}(\text{BO}_3)_x$ series with nominal compositions labelled.

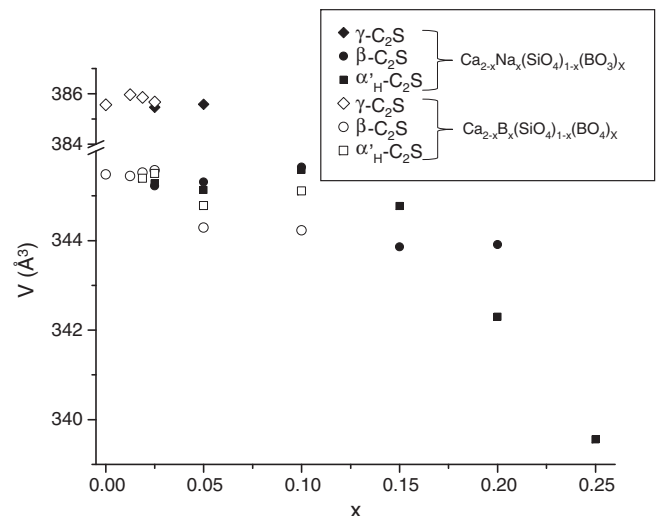


Fig. 4. Variation of the unit cell volumes for $\gamma\text{-C}_2\text{S}$ (rhombus), $\beta\text{-C}_2\text{S}$ (circle) and $\alpha'\text{-H-C}_2\text{S}$ (square) with nominal composition for $\text{Ca}_{2-x}\text{B}_x(\text{SiO}_4)_{1-x}(\text{BO}_4)_x$ (open symbols) and $\text{Ca}_{2-x}\text{Na}_x(\text{SiO}_4)_{1-x}(\text{BO}_3)_x$ (closed symbols) series from Rietveld refinements.

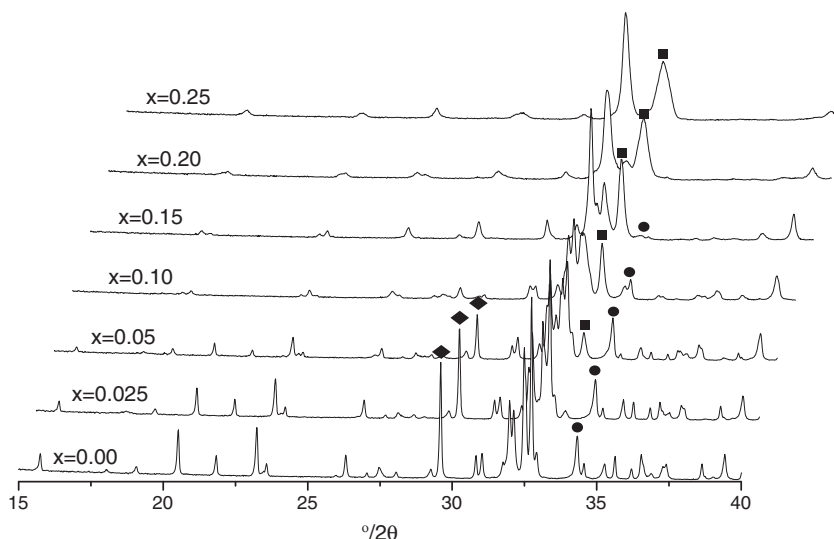


Fig. 5. 3D-view of a selected range of the LXRPD raw patterns for $\text{Ca}_{2-x}\text{Na}_x(\text{SiO}_4)_{1-x}(\text{BO}_3)_x$ solid solution with nominal compositions labelled. Symbols highlight diagnostic peaks for $\gamma\text{-C}_2\text{S}$ (rhombus); $\beta\text{-C}_2\text{S}$ (circle) and $\alpha'\text{-H-C}_2\text{S}$ (square).

For $\text{Ca}_{2-x}\text{Na}_x(\text{SiO}_4)_{1-x}(\text{BO}_3)_x$ series, $\beta\text{-C}_2\text{S}$ is present between $x = 0.00$ and $x = 0.20$. On the other hand, $\alpha'\text{-H-C}_2\text{S}$ appears from $x = 0.025$ up to $x = 0.25$, the last composition being single phase. All powder patterns were analyzed by the Rietveld method. Final refined unit cell parameters of each polymorph and RQPA of all solid solution members are given as supplementary material in Table S3. Fig. 4 plots the variation of the refined unit cell volumes along this series (closed symbols). The same conclusions as with the previous discussed series can be drawn for unit cell volume variations within this one: i) γ -form unit cell volume is constant in its whole chemical field of existence, ii) β - and $\alpha'\text{-H}$ -form unit cell volumes are relatively constant up to $x = 0.10$ and decrease for higher values of x . However, the contraction of unit cell volume in this series occurs at a smaller pace than in the previous studied one, mainly due to the smaller ionic radii mismatch of the Na/Ca when compared to B/Ca. This unit cell contraction has been previously observed in high belite clinkers doped with borax [5]. ATR-FTIR infrared spectra of this series, Fig. 3b, confirms the presence of BO_3^{3-} units and the intensities of their vibration bands, close to 1250 cm^{-1} , increase with x , and the absence of BO_4^{5-} units, as there are not signals around 1000 cm^{-1} .

Fig. 6 displays the ^{11}B ($I = 3/2$) MAS-NMR spectra for three selected samples: BCSAF-B2 clinker, $\text{Ca}_{1.85}\text{Na}_{0.15}(\text{SiO}_4)_{0.85}(\text{BO}_3)_{0.15}$ and $\text{Ca}_{1.90}\text{B}_{0.10}(\text{SiO}_4)_{0.90}(\text{BO}_4)_{0.10}$. This figure also shows, the ^{11}B MAS-NMR spectra (experimental and calculated) for crystalline $\text{B}(\text{OH})_3$ standard taken from reference [56]. This spectrum shows three maxima arising from a unique trigonal-planar BO_3^{3-} group due to the quadrupolar splitting [57]. The ^{11}B MAS-NMR spectra for BCSAF-B2 and $\text{Ca}_{1.85}\text{Na}_{0.15}(\text{SiO}_4)_{0.85}(\text{BO}_3)_{0.15}$ sample are very similar to that of $\text{B}(\text{OH})_3$ and fully consistent with the presence of trigonal BO_3^{3-} groups. The central signal is formed by two maxima at 19 and 8 ppm and a small shoulder at -2 ppm. A second very small additional signal is evident in the spectrum of $\text{Ca}_{1.85}\text{Na}_{0.15}(\text{SiO}_4)_{0.85}(\text{BO}_3)_{0.15}$ sample which may be related to the incorporation of planar BO_3 units in the side-phase, $\beta\text{-C}_2\text{S}$, see Table 2.

The ^{11}B MAS-NMR spectrum for $\text{Ca}_{1.90}\text{B}_{0.10}(\text{SiO}_4)_{0.90}(\text{BO}_4)_{0.10}$ (see Fig. 6 bottom) is more complex in agreement with the infrared data and the charge-compensation mechanism. In addition to at least one (likely two) BO_3 groups, the fitting of the experimental profile requires also the presence of a tetrahedral BO_4^{5-} unit at ~ 0 ppm [58,59]. In any case, it is clear the coexistence of trigonal BO_3^{3-} and tetrahedral

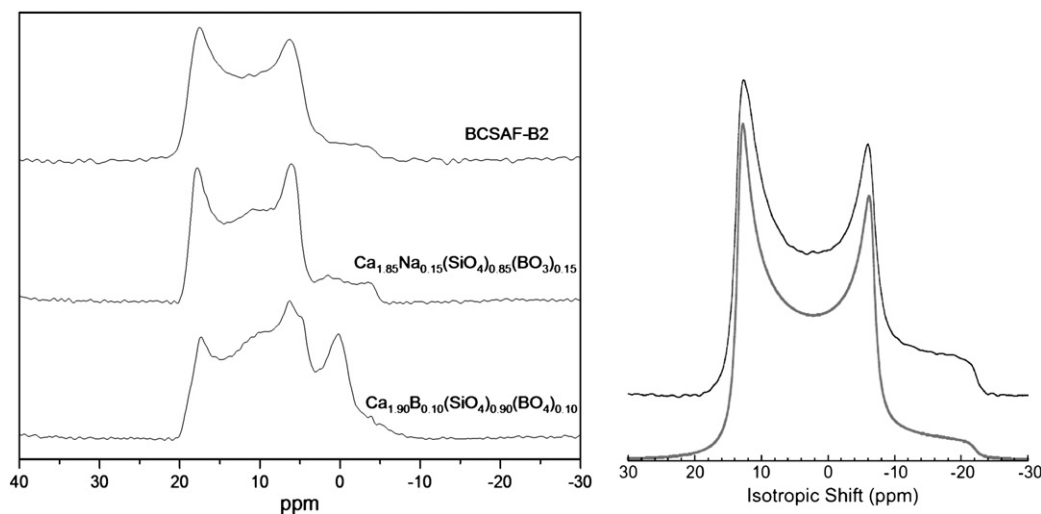


Fig. 6. (Left) ^{11}B MAS NMR spectra for BCSAF-B2 clinker (top), $\text{Ca}_{1.85}\text{Na}_{0.15}(\text{SiO}_4)_{0.85}(\text{BO}_3)_{0.15}$ (intermediate) and $\text{Ca}_{1.90}\text{B}_{0.10}(\text{SiO}_4)_{0.90}(\text{BO}_4)_{0.10}$ (bottom). (Right) For the sake of comparison, it is also shown the ^{11}B MAS-NMR spectrum (experimental and calculated) for crystalline $\text{B}(\text{OH})_3$ from reference [56] which displays a unique trigonal BO_3 group.

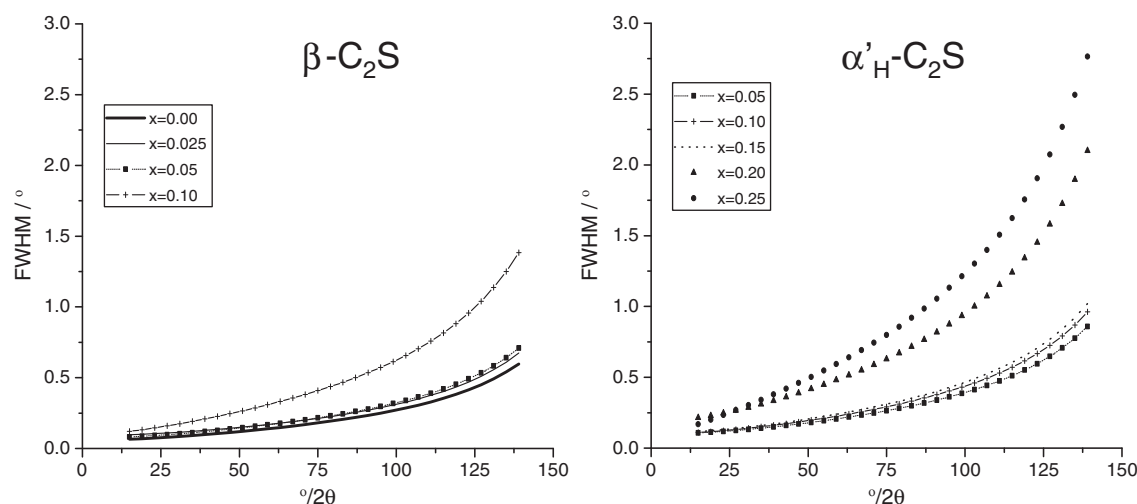


Fig. 7. Variation of FWHM values with diffraction angle (2θ) for β - C_2S (left) and α'_H - C_2S (right) in $Ca_{2-x}Na_x(SiO_4)_{1-x}(BO_3)_x$ series (nominal compositions) obtained from Rietveld refinements using a pseudo-Voigt function.

BO_4^{5-} units for this composition and that the borax-activated BCSAF clinker contains just trigonal BO_3 groups.

The series $Ca_{2-3x}B_{2x}Na_x(SiO_4)_{1-x}(BO_4)_x$ has been also prepared for $0.0 \leq x \leq 0.10$. Sample with $x = 0.10$ was melted at high temperature, thus it was not further studied. Table 2 shows RQPA up to $x = 0.05$. The proposed stoichiometries do not yield to stabilize high temperature polymorphs of dicalcium silicate as high amounts of rankinite [60] ($Ca_3Si_2O_7$) are formed. Thus, this series was ruled out.

Summarising up this section, we must highlight that several solid solutions have been tested but pure belite phases were only formed for the $Ca_{2-x}B_x(SiO_4)_{1-x}(BO_4)_x$ and $Ca_{2-x}Na_x(SiO_4)_{1-x}(BO_3)_x$ solid solutions. However, most of these samples showed co-existence of belite polymorphs.

3.2. Microstructural characterization of $Ca_{2-x}Na_x(SiO_4)_{1-x}(BO_3)_x$

Fig. 5 shows a clear diffraction peak broadening with x , behaviour which was not observed in the remaining series. In order to quantify this evolution, Fig. 7 shows the average full width at the half maximum (FWHM) of the diffraction peaks for the two belite phases (β - and α'_H -forms) as function of the diffraction angle. It can be seen that samples with larger x values present higher FWHM values. This behaviour may be due to (i) small (variable) particle sizes and/or (ii) microstrain evolution. Some members of this series were studied by SEM ($x = 0.10, 0.15$ and 0.20) and the average particle size is almost identical, see Fig. 8. Consequently, peak shape broadening,

mainly for large values of x , is chiefly due to microstrains. These microstrains are likely consequences of the ionic radii mismatch of the B/Si and Na/Ca substitutions. It is interesting to note that there are 'critical' doping values where the broadening increases notably, $x = 0.10$ for β - C_2S and $x = 0.20$ for α'_H - C_2S , see Fig. 7.

On the other hand, it is known that surfaces of dicalcium silicate particles present stripes which seem to be lamella-like waves related to $\alpha' \rightarrow \beta$ conversion [26,61]. However, these effects were not observed in any of the samples containing B_2O_3 and Na_2O , independently of the phase assemblage. This result is in agreement with a previous report from independent authors [43]. In this series, room temperature unit cell volume of β - and α'_H -forms are very similar, and as x increases $V_{\alpha'_H}$ is even smaller than V_β , see Fig. 4. However, in other studies [25] room temperature unit cell volume of α'_H -form is slightly larger (347.5 \AA^3) than that of β - C_2S (345.8 \AA^3). The very small differences between unit cell volumes of β - and α'_H -forms, caused by the addition of borax, is likely a key factor in avoiding the formation of the lamella-like microstructure.

3.3. Crystal structure characterization of α'_H - C_2S

$Ca_{1.85}Na_{0.15}(SiO_4)_{0.85}(BO_3)_{0.15}$ composition was selected to further study the crystal structure of room-temperature stabilized α'_H - C_2S . This choice is based on the trade off between sharp diffraction peaks and the highest content of α'_H -phase. We have used the crystal

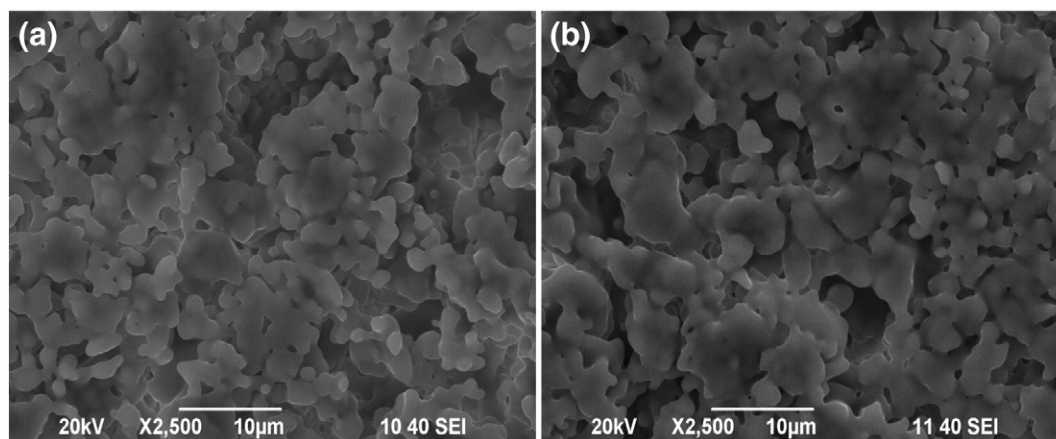


Fig. 8. SEM micrographs of sintered pellets of $Ca_{2-x}Na_x(SiO_4)_{1-x}(BO_3)_x$ [nominal composition: $x = 0.10$ (a) and 0.20 (b)] series.

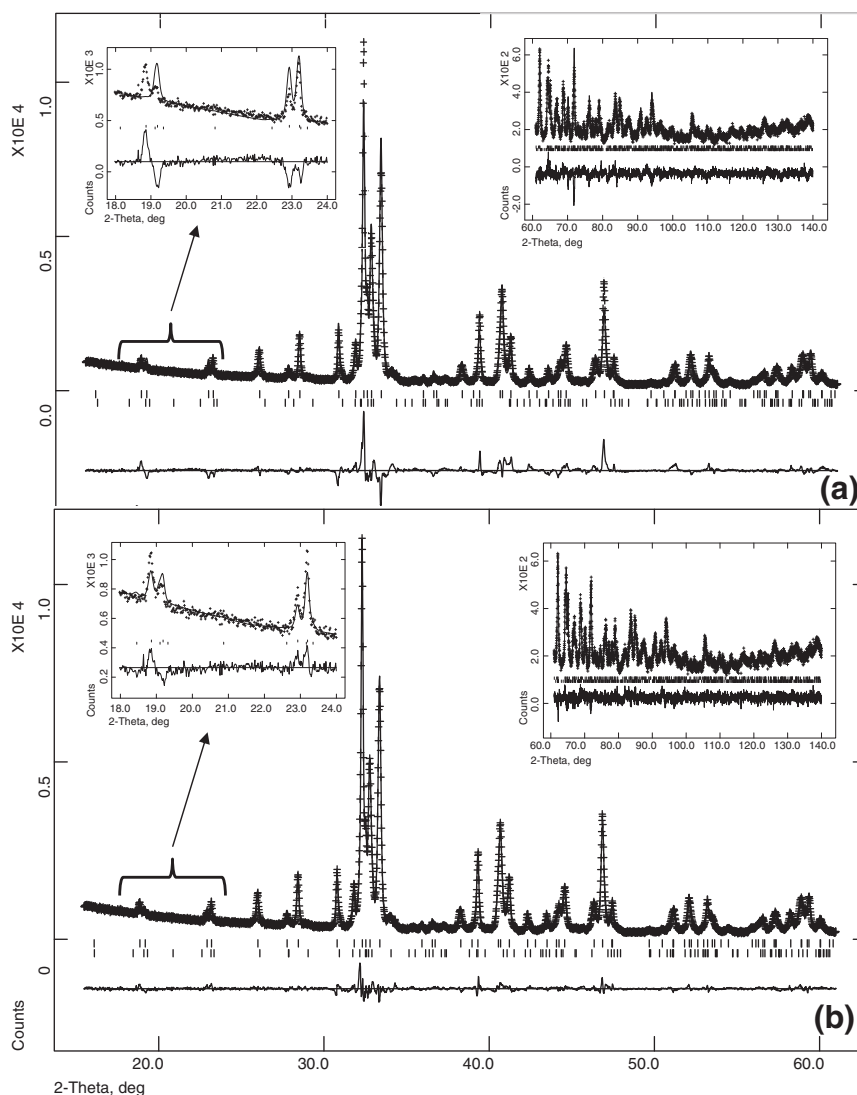


Fig. 9. LXPDP Rietveld plot ($\lambda = 1.5406 \text{ \AA}$) for the sample with nominal composition $\text{Ca}_{1.85}\text{Na}_{0.15}(\text{SiO}_4)_{0.85}(\text{BO}_3)_{0.15}$ (a) using the crystal structure for $\alpha'_\text{H}\text{-C}_2\text{S}$ reported in reference 25 and (b) using the crystal structure reported here. The insets show detailed views of selected low and high angles' regions to highlight the quality of the new fit.

structure description reported by Mumme et al. [25] as a starting model for the Rietveld refinement. After overall parameters optimization, but keeping fixed the structural parameters, the obtained disagreement factors were $R_{\text{WP}} = 10.8\%$ and $R_{\text{F}}(\alpha'_\text{H}\text{-C}_2\text{S}) = 4.1\%$. The typical Rietveld plot is shown in Fig. 9a.

The structural description of $\alpha'_\text{H}\text{-C}_2\text{S}$ polymorph, space group Pnma, has seven crystallographically independent sites in the asymmetric part of the unit cell: 2 Ca's in general position; 1 Si in special position ($x1/4z$); and 4 O in general positions. Moreover, the disorder in the structure is modeled by the occupation factors which are 0.5 for Ca's and O's in stoichiometric $\alpha'_\text{H}\text{-Ca}_2\text{SiO}_4$.

Firstly, and keeping the occupation factors of the stoichiometric phase, the atomic positional parameters were optimized. The refinement converged to chemically realistic interatomic distances, and consequently, soft constraints were not included in the refinement. Secondly, ADPs or Debye-Waller factors were optimized. As some oxygen ADP values became negative, all oxygen ADPs were grouped together. This refinement converged to $R_{\text{WP}} = 6.77\%$ and $R_{\text{F}}(\alpha'_\text{H}\text{-C}_2\text{S}) = 3.02\%$, showing a clear improvement respect to the initial structural description. Finally, nominal cation stoichiometry was included in the refinement by substitution of Ca by Na and Si by B. The occupation factors were kept fixed to the nominal stoichiometry and positional parameters and ADP factors were optimized. The fit was good enough

to refine the oxygen ADPs independently, without any negative Debye-Waller factor. The final key R-factors were to $R_{\text{WP}} = 6.52\%$ and $R_{\text{F}}(\alpha'_\text{H}\text{-C}_2\text{S}) = 2.37\%$. Fig. 9b gives the fit for this last refinement. Fig. 9 also includes an enlarged view of two selected regions (low and high angle ranges) to highlight the improvement in the fit with the final structural description.

Table 3

Refined atom positions and atomic displacement parameters (ADPs) for $\alpha'_\text{H}\text{-C}_2\text{S}$ in the sample $\text{Ca}_{2-x}\text{Na}_x(\text{SiO}_4)_{1-x}(\text{BO}_3)_x$ with $x = 0.15$. Space group: Pnma. Refined unit cell: $a = 6.8432(2) \text{ \AA}$, $b = 5.4555(1) \text{ \AA}$ and $c = 9.2346(2) \text{ \AA}$.

Atom	x	y	z	S.O.F.*	ADPs / \AA^2
Ca1, 8 d	0.3270(2)	0.2850(8)	0.5702(2)	0.4625	0.0260(7)
Na1, 8 d	0.3270(2)	0.2850(8)	0.5702(2)	0.0375	0.0260(7)
Ca2, 8 d	0.9912(2)	0.2709(9)	0.2938(1)	0.4625	0.0107(6)
Na2, 8 d	0.9912(2)	0.2709(9)	0.2938(1)	0.0375	0.0107(6)
O1, 8 d	1.0027(7)	0.3247(11)	0.5427(5)	0.5000	0.0374(22)
O2, 8 d	0.7555(8)	0.0258(10)	0.7086(7)	0.5000	0.0055(20)
O3, 8 d	0.6517(7)	0.1838(13)	0.4439(5)	0.5000	0.0279(19)
O4, 8 d	0.6973(9)	0.4868(13)	0.6600(7)	0.5000	0.0182(23)
Si1, 4c	0.7745(3)	0.2500	0.5901(3)	0.8500	0.0175(7)
B, 4c	0.7745(3)	0.2500	0.5901(3)	0.1500	0.0175(7)

*Space occupation factor.

Table 4

Rietveld quantitative phase analyses, expressed in weight percentages, for a doped BCSA clinker, using the refined structure description for $\alpha'_H\text{-C}_2\text{S}$ (upper row) and the Mumme et al. structure [25] (italics). R_{WP} and R_F for $\alpha'_H\text{-C}_2\text{S}$ agreement factors are also included.

$\alpha'_H\text{-C}_2\text{S}$	$R_F(\alpha'_H)$ (%)	$\text{Ca}_4\text{Al}_6\text{O}_{12}\text{SO}_4$	$\text{Ca}_2\text{AlFeO}_5$	R_{WP} (%)
58.3(2)	4.36	29.4(1)	12.3(2)	4.77
53.7(2)	5.41	32.1(2)	14.2(2)	5.21

Refined atomic positional parameters and isotropic atomic displacement factors are given in Table 3, and also deposited as a CIF file for RQPA. The final refined unit cell parameters for $\alpha'_H\text{-Ca}_{1.85}\text{Na}_{0.15}(\text{SiO}_4)_{0.85}(\text{BO}_3)_{0.15}$ were $a = 6.8432(2)$ Å, $b = 5.4555(1)$ Å, $c = 9.2346(2)$ Å and $V = 344.76(2)$ Å³. It is worth mentioning that the phase composition was fixed to the nominal starting cation stoichiometry. However, the oxygen disorder induced by the borate incorporation has not been modelled and neutron powder diffraction is needed to address this feature. The disorder in the SiO_4^{4-} units is large and similar to that already reported [25]. Finally, it is also worth noting that this sample contains 90.1(1) wt% of $\alpha'_H\text{-C}_2\text{S}$ and 9.9(2) wt% of $\beta\text{-C}_2\text{S}$.

This structural description was used to perform RQPA of the remaining members of all the series containing $\alpha'_H\text{-C}_2\text{S}$, Table 2. Furthermore, this structural description has been used to quantify this phase in belite calcium sulfoaluminate (BCSA) clinkers doped with 2.0 wt% of B_2O_3 , added as borax [5]. This clinker contains three main phases, $\alpha'_H\text{-C}_2\text{S}$, cubic [62] $\text{Ca}_4\text{Al}_6\text{O}_{12}\text{SO}_4$ (also called Klein salt or ye'elimite) and orthorhombic [63] $\text{Ca}_2\text{AlFeO}_5$. RQPA was performed for this clinker by using the refined crystal structure for $\alpha'_H\text{-C}_2\text{S}$ obtained in this report (Figure S3b) and the Mumme et al. structure [25] (Figure S3a), using exactly the same refinement strategies. Table 4 includes RQPA of doped BCSA clinker being $\alpha'_H\text{-C}_2\text{S}$ fitted by the refined crystal description of this work (upper row) and with crystal structure published by Mumme et al. [25] It is observed how agreement indices (R_{WP} and R_F for $\alpha'_H\text{-C}_2\text{S}$) are lower, i.e. means better fits, when using the refined crystal structure for α'_H -form and consequently, the weight percentage of this phase has increased. We have evaluated the refined unit cell parameters of this $\alpha'_H\text{-C}_2\text{S}$ included in a BCSA clinker: $a = 6.8263(3)$ Å, $b = 5.4684(3)$ Å, $c = 9.2658(4)$ Å and volume = 345.88(4) Å³. Taking into account this refined volume, it can be assessed that the $\alpha'_H\text{-C}_2\text{S}$ stabilized in a BCSA clinker by adding 2 wt% of B_2O_3 , added as borax, may have a stoichiometry close to $x = 0.10$, see Fig. 4, using the $\text{Ca}_{2-x}\text{Na}_x(\text{SiO}_4)_{1-x}(\text{BO}_3)_x$ mechanism. Finally, the influence of polymorphism and microstructure in the kinetic of the C_2S hydration are being studied and the results will be reported elsewhere.

4. Conclusions

The boron and sodium/boron doping of dicalcium silicate has been investigated. In order to understand the substitution of silicon by boron, three solid solutions have been tested: $\text{Ca}_{2-x/2}\text{Na}_{x/2}(\text{SiO}_4)_{1-x}(\text{BO}_3)_x$, $\text{Ca}_2(\text{SiO}_4)_{1-x}(\text{BO}_3)_x\text{O}_{x/2}$ and $\text{Ca}_{2-x}\text{B}_x(\text{SiO}_4)_{1-x}(\text{BO}_4)_x$. The experimental results, in the reported synthetic conditions, support the formation of the $\text{Ca}_{2-x}\text{B}_x(\text{SiO}_4)_{1-x}(\text{BO}_4)_x$ series. This doping mechanism similar to that already reported for aluminum doping calcium silicates. On the other hand, the coupled sodium/boron doping of belite has also been investigated by the preparation of two series: $\text{Ca}_{2-x}\text{Na}_x(\text{SiO}_4)_{1-x}(\text{BO}_3)_x$ and $\text{Ca}_{2-3x}\text{B}_{2x}\text{Na}_x(\text{SiO}_4)_{1-x}(\text{BO}_4)_x$. $\text{Ca}_{2-x}\text{Na}_x(\text{SiO}_4)_{1-x}(\text{BO}_3)_x$ series is formed and $\alpha'_H\text{-C}_2\text{S}$ is the main phase for x values larger than 0.10 and it is single phase for $x = 0.25$. Therefore, boron substitutes silicon as tetrahedral borate anion, BO_3^{3-} , for single-boron doping; but as triangular-planar anion, BO_3^{3-} , for coupled boron and sodium doping. Finally, a new structural description for Na/B doping in belite has been developed for $\alpha'_H\text{-Ca}_{1.85}\text{Na}_{0.15}(\text{SiO}_4)_{0.85}(\text{BO}_3)_{0.15}$. This structure fits better

cement samples including reactive belite prepared by borax addition. This behaviour has also been confirmed by ¹¹B MAS NMR as the borax-activated iron-rich belite calcium sulfoaluminate clinker displays a spectrum typical of trigonal-planar BO_3 groups.

Acknowledgment

This work has been supported by Spanish Ministry of Science and Innovation through MAT2010-16213 research grant which is co-funded by FEDER.

Appendix A. Supplementary data

Supplementary data to this article can be found online at doi:10.1016/j.cemconres.2012.01.006.

References

- [1] D. Gielen, K. Tanaka, Energy efficiency and CO₂ emission reduction potentials and policies in the cement industry: towards a plan of action, Proceedings of the IEA/WBCSD Workshop on Energy Efficiency and CO₂ Emission Reduction Potentials and Policies in the Cement Industry, Paris, 4–5 September 2006, International Energy Agency, Paris, 2007. http://www.iea.org/work/workshopdetail.asp?WS_ID=266.
- [2] A.K. Chatterjee, High Belite Cements—Present Status and Future Technological Options: Part I, Cem. Concr. Res. 26 (1996) 1213–1225.
- [3] A. Guerrero, S. Goñi, I. Campillo, A. Moragues, Belite Cement Clinker from Coal Fly Ash of High Ca Content. Optimization of Synthesis Parameters, Environ. Sci. Technol. 38 (2004) 3209–3213.
- [4] A.G. De la Torre, M.A.G. Aranda, A.H. De Aza, P. Pena, S. De Aza, Belite Portland Clinkers. Synthesis and Mineralogical Analysis, Bol. Soc. Esp. Ceram. Vidrio 44 (2005) 185–191.
- [5] A.J.M. Cuberos, A.G. De la Torre, G. Álvarez-Pinazo, M.C. Martín-Sedeño, K. Schollbach, H. Pöllmann, M.A.G. Aranda, Active Iron-Rich Belite Sulfoaluminate Cements: Clinkering and Hydration, Environ. Sci. Technol. 44 (2010) 6855–6862.
- [6] K. Quillin, Calcium sulfoaluminate cements, CO₂ reduction, concrete properties and applications, IHS BRE press, 2007.
- [7] E. Gartner, Industrially interesting approaches to “low-CO₂” cements, Cem. Concr. Res. 34 (2004) 1489–1498.
- [8] C.D. Popescu, M. Muntean, J.H. Sharp, Production of Low Energy Belite Cement, Cem. Concr. Composites 25 (2003) 689–693.
- [9] L. Zhang, M. Su, Y. Wang, Development and Use of Sulpho- and Ferro-aluminate cements in China, Adv. Cem. Res. 11 (1999) 15–21.
- [10] H.F.W. Taylor, Cement Chemistry, second ed. Thomas Telford, London, 1997.
- [11] S.N. Ghosh, P.B. Rao, A.K. Paul, K.J. Raina, The chemistry of the dicalcium silicate mineral, Mater. Sci. 14 (1979) 1554–1566.
- [12] M. Regourd, M. Bigare, J. Forest, A. Guinier, Synthesis and Crystallographic Investigation of Some Belites, Proceedings of the 5th International Symposium on the Chemistry of Cement, Part I, Supplement Paper I-10, Tokyo, 1968, pp. 44–48.
- [13] D.K. Smith, A. Majumdar, F. Ordway, The crystal structure of [gamma]-dicalcium silicate, Acta Crystallogr. 18 (1965) 787–795.
- [14] R. Czaya, Refinement of the structure of $\text{-Ca}_2\text{SiO}_4$, Acta Crystallogr., Sect. B: Struct. Sci 27 (1971) 848–849.
- [15] S. Udagawa, K. Urabe, M. Natsume, T. Yano, Refinement of the crystal structure of $\gamma\text{-Ca}_2\text{SiO}_4$, Cem. Concr. Res. 10 (1980) 139–144.
- [16] C.M. Midgley, The crystal structure of β dicalcium silicate, Acta Crystallogr. 5 (1952) 307–312.
- [17] K.H. Jost, B. Ziemer, R. Seydel, Redetermination of the structure of β -dicalcium silicate, Acta Crystallogr., Sect. B: Struct. Sci 33 (1977) 1696–1700.
- [18] K. Susuki, G. Yamaguchi, A Structural Study on $\alpha'\text{-Ca}_2\text{SiO}_4$, Supplement Paper, Tokyo, Proceedings of the 5th International Symposium on the Chemistry of Cement, 1968, pp. 67–72.
- [19] P. Barnes, C.H. Fentiman, J.W. Jeffery, Structurally related dicalcium silicate phases, Acta Crystallogr., Sect. A: Found. Crystallogr. 36 (1980) 353–356.
- [20] H. Saalfeld, X-Ray Investigation of Single Crystals of $\beta\text{-Ca}_2\text{SiO}_4$ (Larnite) at High Temperatures, Am. Mineral. 60 (1975) 824–827.
- [21] I. Jelenic, A. Bezjak, Electron Diffraction Evidence for Superstructures in β -Modification of Dicalcium Silicate, Cem. Concr. Res. 12 (1982) 785–788.
- [22] A.M. Il'inets, M.Y. Bikbaev, Structural Mechanism of Polymorphic Transitions of Dicalcium Silicate, Ca_2SiO_4 . Part II: Refinement of Crystal Structure of High-Temperature α'_L . Modification of Dicalcium Silicate Ca_2SiO_4 , Kristallografiya 35 (1990) 91–93.
- [23] M.A. Bredig, Polymorphism of calcium orthosilicate, J. Am. Ceram. Soc. 33 (1950) 188–192.
- [24] W. Eysel, T. Hahn, Polymorphism and solid solution of Ca_2GeO_4 and Ca_2SiO_4 , Z. Kristallogr. 131 (1970) 322–341.
- [25] W.G. Mumme, R.J. Hill, G. Bushnell-Wye, E.R.N. Segnit, Rietveld Crystal structure refinements, crystal chemistry and calculated powder diffraction data for the polymorphs of dicalcium silicate and related phases, J. Bone Miner. Abh. 169 (1995) 35–68.

- [26] Y.J. Kim, I. Nettlehip, W.M. Kriven, Phase Transformations in Dicalcium Silicate. II: TEM Studies of Crystallography, Microstructures and Mechanisms, *J. Am. Ceram. Soc.* 75 (1992) 2407–2419.
- [27] Y.-M. Kim, S.-H. Hong, Influence of minor ions on the stability and hydration rates of β -dicalcium silicate, *J. Am. Ceram. Soc.* 87 (2004) 900–905.
- [28] I. Jelenic, A. Bezjak, M. Bujan, Hydration of B_2O_3 -stabilized α' - and β -modifications of dicalcium silicate, *Cem. Concr. Res.* 8 (1978) 173–180.
- [29] D.L. Kantro, C.H. Weise, Hydration of various beta-dicalcium silicate preparations, *J. Am. Ceram. Soc.* 62 (1979) 621–626.
- [30] I. Jelenic, A. Bezjak, On the hydration kinetics of α' - and β -modifications of dicalcium silicate, *Cem. Concr. Res.* 11 (1981) 467–472.
- [31] H. Manzano, E. Durgun, M.J.A. Qomi, F.J. Ulm, R.J.M. Pellenq, J.C. Grossman, Impact of chemical impurities on the crystalline cement clinker phases determined by atomistic simulations, *Cryst. Growth Des.* 11 (2011) 2964–2972.
- [32] I. Nettlehip, K.G. Slavick, Y.J. Kim, W.M. Kriven, Phase transformation in dicalcium silicate: I, Fabrication and phase stability of fine-grained β -phase, *J. Am. Ceram. Soc.* 75 (1992) 2400–2406.
- [33] B. Henderson, Defects in crystalline Solids, Edward Arnold, London, 1972.
- [34] K. Fukuda, S. Ito, Improvement in reactivity and grindability of belite-Rich cement by remelting reaction, *J. Am. Ceram. Soc.* 82 (1999) 2177–2180.
- [35] M. Pritts, K.E. Daugherty, The effect on stabilizing agents on the hydration rate of β - C_2S , *Cem. Concr. Res.* 6 (1976) 783–796.
- [36] B. Matkovic, V. Carin, T. Gacesa, R. Halle, I. Jelenic, J.F. Young, Influence of $BaSO_4$ on the Formation and Hydration Properties of Calcium Silicates: I, Doped Dicalcium Silicates, *Am. Ceram. Soc. Bull.* 60 (1981) 825–829.
- [37] P. Fierens, J. Tirlocq, Nature and concentration effect of stabilizing elements of Beta-dicalcium silicate on its hydration rate, *Cem. Concr. Res.* 13 (1983) 267–276.
- [38] B. Ziemer, B. Altrichter, V. Jesenak, Effect of SO_3 on formation and hydraulic reactivity of belite, *Cem. Concr. Res.* 14 (1984) 686–692.
- [39] My.Y. Benarchid, A. Diouri, A. Boukhari, J. Aride, J. Rogez, R. Castanet, Elaboration and thermal study of iron-phosphorus-substituted dicalcium silicate phase, *Cem. Concr. Res.* 34 (2004) 1873–1879.
- [40] J. Bensted, Some hydration studies of α -dicalcium silicate, *Cem. Concr. Res.* 9 (1979) 97–101.
- [41] K. Fukuda, A. Takeda, H. Yoshida, Remelting reaction of α - Ca_2SiO_4 solid solution confirmed in Ca_2SiO_4 - $Ca_{12}Al_{14}O_{33}$ pseudobinary system, *Cem. Concr. Res.* 31 (2001) 1185–1189.
- [42] A. Wesselsky, O.M. Jensen, Synthesis of pure Portland cement phases, *Cem. Concr. Res.* 39 (2009) 973–980.
- [43] C.K. Park, Phase transformation and hydration of dicalcium silicate containing stabilizers, *J. Ceram. Soc. Jpn.* 109 (2001) 380–386.
- [44] K. Morsli, A.G. De la Torre, S. Stöber, A.J.M. Cuberos, M. Zahir, M.A.G. Aranda, Quantitative phase Analysis of Laboratory-Active Belite Clinkers by Synchrotron Powder Diffraction, *J. Am. Ceram. Soc.* 90 (2007) 3205–3212.
- [45] K. Morsli, A.G. De la Torre, M. Zahir, M.A.G. Aranda, Mineralogical phase analysis of alkali and sulfate bearing belite rich laboratory clinkers, *Cem. Concr. Res.* 37 (2007) 639–646.
- [46] A.C. Larson, R.B. Von Dreele, General Structure Analysis System (GSAS) program. Rep. No. LA-UR-86748, Los Alamos National Laboratory, Los Alamos, CA, 1994.
- [47] P. Thompson, D.E. Cox, J.B. Hasting, Rietveld refinement of Debye-Scherrer synchrotron X-ray data from Al_2O_3 , *J. Appl. Crystallogr.* 20 (1987) 79–83.
- [48] L.W. Finger, D.E. Cox, A.P. Jephcoat, A Correction for Powder Diffraction Peak Asymmetry due to Axial Divergence, *J. Appl. Crystallogr.* 27 (1994) 892–900.
- [49] L. León-Reina, E.R. Losilla, M. Martínez-Lara, S. Bruque, M.A.G. Aranda, Interstitial oxygen conduction in lanthanum oxy-apatite electrolytes, *J. Mater. Chem.* 14 (2004) 1142–1149.
- [50] M. Tukka, J. Hölsä, M. Lastusaari, J. Niittykoski, Eu^{3+} doped rare earth orthoborates, RBO_3 ($R = Y, La$ and Gd), obtained by combustion synthesis, *Opt. Mater.* 27 (2005) 1516–1522.
- [51] A.M. Heyns, K.-J. Range, M. Wildenauer, The vibrational spectra of $NbBO_4$, $TaBO_4$, $NaNb_3O_8$ and $NaTa_3O_8$, *Spectrochim. Acta* 46A (1990) 1621–1628.
- [52] J.M. Porras-Vázquez, A.G. De la Torre, E.R. Losilla, M.A.G. Aranda, Oxide and proton conductivity in aluminium-doped tricalcium oxy-silicate, *Solid State Ionics* 178 (2007) 1073–1080.
- [53] W.-H. Chae, D.-C. Park, S.-H. Choi, Early hydration of modified belite cement prepared by adding borax, *Korean J. Ceram.* 2 (1996) 147–151.
- [54] G.S. Li, E.M. Gartner, High-belite sulfoaluminate clinker: fabrication process and binder preparation, French patent application 04-51586, 2006 (publication 2873366), 27/01/2006.
- [55] G.S. Li, G. Walenta, E.M. Gartner, Formation and hydration of low- CO_2 cements based on belite, calcium sulfoaluminate and calcium aluminoferrite, *Proceedings of the 12th International Congress of the Cements Chemistry, Montreal, 2007*, p. TH3 15.3.
- [56] K. Klochko, G.D. Cody, J.A. Tossell, P. Dera, A.J. Kaufman, Re-evaluating boron speciation in biogenic calcite and aragonite using ^{11}B MAS NMR, *Geochim. Cosmochim. Acta* 73 (2009) 1890–1900.
- [57] A.H. Silver, P.J. Bray, Nuclear Magnetic Resonance Absorption in Glass. I. Nuclear Quadrupole Effects in Boron Oxide, Soda-Boric Oxide, and Borosilicate Glasses, *J. Chem. Phys.* 29 (1958) 984–990.
- [58] M.R. Hansen, G.K.H. Madsen, H.J. Jakobsen, J. Skibsted, Refinement of Borate Structures from ^{11}B MAS NMR Spectroscopy and Density Functional Theory Calculations of ^{11}B Electric Field Gradients, *J. Phys. Chem. A* 109 (2005) 1989–1997.
- [59] S. Kroeker, J.F. Stebbins, Three-Coordinated Boron-11 Chemical Shifts in Borates, *Inorg. Chem.* 40 (2001) 6239–6246.
- [60] I. Kusachi, C. Henmi, A. Kawahara, K. Henmi, The structure of Rankinite, *Mineral. J.* 8 (1975) 38–47 (Japan).
- [61] D.H. Campbell, Microscopical examination and interpretation of Portland cement and clinker: Portland Cement Association, Old Orchard RD, Skokie, USA, 1999.
- [62] H. Saalfeld, W. Depmeier, Silicon-Free compounds with sodalite structure, *Krist. Tech.* 7 (1972) 229–233.
- [63] A.A. Colville, S. Geller, The crystal structure of brownmillerite, Ca_2FeAlO_5 , *Acta Crystallogr. B* 27 (1971) 2311–2315.